THE ROYAL SOCIETY

Sub-inertial dynamics of density-driven flows in a continuously stratified fluid on a sloping bottom. II. Isolated eddies and radiating cold domes

BY FRANCIS J. POULIN AND GORDON E. SWATERS

Applied Mathematics Institute, Department of Mathematical Sciences, University of Alberta, Edmonton, Alberta, Canada T6G 2G1

Received 10 December 1997; accepted 27 October 1998

Dynamical properties of propagating baroclinic bottom-intensified eddies on a sloping bottom are investigated. The model is based on one previously introduced describing the sub-inertial dynamics of density-driven flows on a sloping bottom within a continuously stratified rotating fluid. A variational principle is established for arbitrary nonlinear steadily travelling eddies. Explicit solutions are obtained for fully nonlinear radially symmetric eddies. The eddies correspond to a bottom-trapped cold dome that has a predominantly anticyclonic circulation within it and a relatively strong cyclonic eddy in the overlying fluid, which satisfies the *Mory–Stern* isolation constraint. These eddies are able to transport bottom- and intermediate-water fluid parcels. An approximate solution is also constructed for a radiating cold dome. These eddies possess a topographic Rossby wave field behind the travelling eddy. The associated wave drag results in down-slope motion into deeper waters. The theoretical work is illustrated with a specific solution for a cold dome with a parabolic height profile that intersects the bottom.

Keywords: oceanographic eddies and vortices; density-driven currents; physical oceanography

1. Introduction

This paper is a continuation of Poulin & Swaters (1999), hereafter referred to as part I. In that paper, a new model was introduced describing the sub-inertial dynamics of density-driven currents within a continuously stratified rotating fluid over sloping topography. The principal purpose of part I was to describe the underlying dynamical balances of the theory and to provide a comprehensive stability analysis of steady solutions to the model. Here, our goal is to describe the properties of isolated eddy and radiating cold-dome solutions to the model.

Briefly, the model corresponds to a two-fluid configuration in which the lower layer, or density-driven current, is described by geostrophically balanced shallow-water dynamics over sloping topography, which allows for finite-amplitude thickness variations. The upper layer, which is continuously stratified, is described by quasi-geostrophic dynamics in which the velocity field is principally driven by a baroclinic vortex-tube stretching associated with deformations in the lower-layer height and a background topographic vorticity gradient.

© 1999 The Royal Society
TEX Paper

From the point of view of the instability process, the model filters out barotropic destabilization within the lower layer and focuses on the baroclinic dynamics. Because these geostrophically balanced flows on a sloping bottom are driven by the density contrast with the surrounding water we refer to them as 'mesoscale gravity currents' (see, for example, Britter & Linden 1980; Honji & Hosoyamada 1989; LeBlond *et al.* 1991) in order to emphasize the underlying fluid dynamical configuration and to differentiate them from non-rotating gravity currents on a flat bottom.

The eddies we describe here correspond to propagating bottom-intensified baroclinic vortices. Within the lower layer, the eddies correspond to cold domes with a primarily anticyclonic circulation. Within the upper layer, the eddies have cyclonic circulation that is most intense immediately above the cold dome (but which can extend throughout the water column). From the theoretical point of view, the solutions we present here are extensions of the reduced-gravity cold domes described by Nof (1983) and the two-layer eddies described by Swaters & Flierl (1991).

Density-driven baroclinic eddies are common features associated with the destabilization of mesoscale gravity currents such as overflows in continental seas. Numerical simulations of overflows (see, for example, Jiang & Garwood 1996; Swaters 1998*a*) show the formation of bottom-intensified density-driven eddies resulting from the baroclinic instability (Swaters 1991) of these currents. Analysis of IR satellite imagery (Bruce 1995) has shown the formation and propagation of eddies associated with, for example, the Denmark Strait overflow. These eddies, which extend vertically throughout the water column, have radii of the order of 20–40 km and lifetimes of at least 30 days. Bruce (1995) concluded that the formation of the eddies was correlated with vortex stretching associated with deep-water pulses flowing over the sill of the Denmark Strait. Houghton *et al.* (1982) also observed the formation and alongslope propagation of a cold dome on the New England Bight. This cold dome had a cross-shelf length-scale of *ca.* 10–15 km and a lifetime in excess of several months.

In addition, laboratory experiments have also shown the formation of these bottom-intensified eddies associated with density-driven currents (see, for example, Mory *et al.* 1987; Honji & Hosoyamada 1989; Whitehead *et al.* 1990). One of the most important observations made by Mory *et al.* (1987) and Honji & Hosoyamada (1989) was that there was an appreciable azimuthal cyclonic velocity field formed in the fluid over the cold dome.

In the case where the eddy is isolated, i.e. there is no external wave field coupled to the eddy, Mory (1985) and Mory *et al.* (1987) showed, based on a two-layer shallow-water model, that the sum of the dynamic height anomaly in the overlying fluid and the lower-layer height must integrate to zero. Since the height or thickness associated with a cold dome is everywhere non-negative, this constraint, which we call the *Mory–Stern isolation constraint* (in our context see (3.5)), implies that the dynamic pressure in the overlying fluid must be predominantly negative, which gives rise to strong cyclonic circulation overlying the cold dome.

Indeed, this overlying circulation can be strong enough that there will be closed isolines of the co-moving stream function (Swaters 1998*a*), i.e. the eddy can transport upper-layer fluid parcels. Thus, these cold domes cannot only play a role in the mass/heat flux of bottom waters along continental slopes, they can also help to distribute intermediate and upper waters as well. We believe that the balances examined here are relevant for understanding the dynamics of benthic currents associated with the thermohaline circulation in the oceans.

If the Mory–Stern isolation constraint is not satisfied, then the eddy will radiate energy away via (topographic) Rossby waves (Swaters 1998*b*). However, the time-scale over which this decay takes place is much longer than the eddy-circulation time-scale (see, for example, Flierl 1984). Numerical simulations (Swaters 1998*a*) show that even in this case the eddies remain remarkably coherent over many eddy-circulation times (e.g. 200–300 days). Thus, it seems that these density-driven vortices are rather robust flow features. It is of interest, therefore, to develop models that can accurately describe their internal dynamics and their interaction with the surrounding ocean.

Nof (1983) developed a reduced-gravity or equivalent barotropic model for the propagation characteristics of cold domes on a linearly sloping bottom. Perhaps the most important conclusion obtained by Nof (1983) was that the velocity of a cold dome with compact support (i.e. an eddy that extends over a finite horizontal area) was oriented solely in the along-slope direction with magnitude $g's^*/f$, which we call the *Nof speed*, where g', s^* and f are the reduced gravity, the bottom slope and the local Coriolis parameter, respectively. The importance of Nof's result is that it suggests that the propagation velocity is independent of the spatial and vorticity characteristics of the cold dome.

One of the principal weaknesses associated with Nof's (1983) model is that it does not include any dynamical interaction with the surrounding fluid, which the laboratory experiments cited above and the Mory–Stern isolation constraint suggest cannot be neglected. In general, the interaction between a cold dome and the surrounding fluid will modify the along-slope velocity as predicted by Nof (1983) and lead to a cross-slope drift (see, for example, Swaters & Flierl 1991). The cross-slope drift is the geostrophic response of the eddy to the drag associated with an external topographic Rossby wave field. However, if the Mory–Stern isolation constraint is satisfied by the eddy/surrounding water configuration, i.e. no external topographic Rossby wave field exists, then the baroclinic cold dome travels at the Nof velocity *and* a strong cyclonic circulation occurs over the cold dome. We hasten to add, of course, that there are other physical processes that can lead to a cross-slope drift, such as, for example, bottom friction.

The plan of this paper is as follows. In the remainder of this section we very briefly describe the model equations. In § 2 we present a general description, including a variational principle, for arbitrary nonlinear steadily travelling eddy solutions of the model. In § 3 we examine fully nonlinear radially symmetric eddies. An exact general solution is presented. The physically necessary imposition of a zero upstream waves condition leads to the complete elimination of any external wave field for these eddies. We show that these eddies travel with the Nof velocity and satisfy the analogue of the Mory–Stern isolation constraint (which leads to a quantization of the allowed eddy radii). The spatial characteristics are illustrated for a simple eddy height that is parabolic in shape. In § 4 we present an asymptotic solution for a radiating eddy that possesses a topographic Rossby wave field in the far field behind the propagating eddy (which, nevertheless, satisfies the zero upstream waves condition). The Rossby wave field results in the down-slope motion of the eddy, i.e. the overall motion is 'southwestward' relative to the topographic β-plane.

(*a*) *Governing equations*

The notation used here is identical to that introduced in part I, and the reader is referred there for a complete description. If the geostrophic pressure in the upper

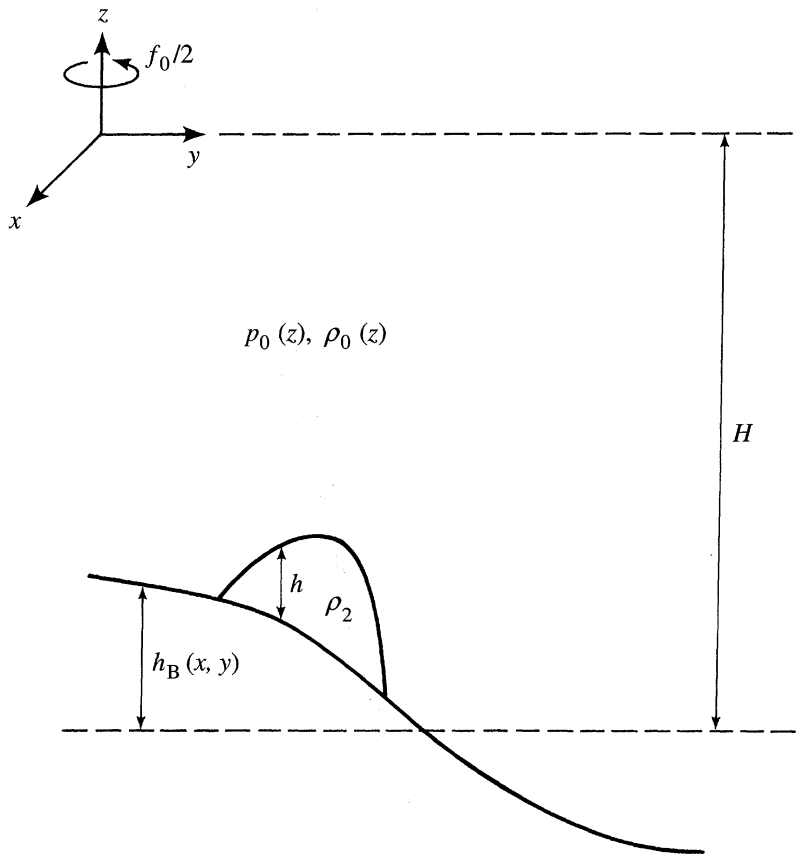

Figure 1. Geometry of the model used in this paper.

continuously stratified layer is denoted by $\varphi(x, y, z, t)$ and the lower-layer height by $h(x, y, t)$, where (x, y) and z are the right-handed horizontal and vertical coordinates, respectively, and where the bottom topography is denoted by $h_B(x, y)$ (see figure 1), the non-dimensional model equations can be written in the form

$$\partial_t[\Delta\varphi + (N^{-2}\varphi_z)_z] + \mu J(\varphi, \Delta\varphi + (N^{-2}\varphi_z)_z) = 0, \tag{1.1}$$

with the vertical boundary conditions

$$\varphi_{zt} + \mu J(\varphi, \varphi_z) = 0, \quad \text{on } z = 0, \tag{1.2}$$

$$\varphi_{zt} + \mu J(\varphi, \varphi_z) + N^2 J(\varphi + h, h_B) = 0, \quad \text{on } z = -1, \tag{1.3}$$

$$h_t + J(\mu\varphi + h_B, h) = 0, \quad \text{on } z = -1. \tag{1.4}$$

The parameter $N(z)$ is the non-dimensional Brunt–Väisälä frequency associated with the upper layer, which is assumed to be stably stratified. We refer to the parameter μ in the model as the *interaction parameter*, and it is defined by (see part I)

$$\mu = [\delta/s] \simeq O(1),$$

where

$$\delta = \frac{h_*}{H} \quad \text{and} \quad s = \frac{g's^*/f}{\sqrt{g'H}},$$

where h_* and H are representative dimensional values for the lower-layer height and upper-layer depth, respectively, and s^* is a typical value for the bottom slope or gradient. In this paper, h_* is taken to be the maximum height of the lower-layer cold dome (see figure 1).

The interaction parameter is a measure of the ratio of the role of vortex tube stretching to the background topographic vorticity gradient. With respect to the dynamics of the lower layer, i.e. (1.4), it is a measure of the coupling between the two layers. In the upper-layer equations, it is a measure of the nonlinearity of the flow. From the point of view of the instability problem, μ is the key instability parameter in the sense that it represents the ratio of the destabilizing effect of baroclinicity to the stabilizing effect of the topographic slope. That is, increasing μ destabilizes an otherwise stable flow (see part I and Swaters 1991).

The model equations are derived assuming $0 < s \ll 1$ (see part I). The parameter s is the ratio of the Nof speed to the speed of long or irrotational internal gravity waves in a reduced-gravity model. The small s limit may be thought of as filtering out the higher-frequency dynamics associated with non-rotating gravity currents and focusing on the rotationally dominated aspects of the problem. Alternatively, a small s limit may be thought of as a sub-inertial approximation in which the horizontal length-scale is larger than the internal deformation radius associated with the lower layer (i.e. an intermediate length-scale approximation in the sense of, for example, Charney & Flierl (1981)). Swaters & Flierl (1991), based on data from Houghton *et al.* (1982), estimate $s \simeq O(10^{-2})$ and $\mu \simeq 2$ as typical for the cold dome observed on the New England Bight. Similar estimates occur for other gravity-driven flows we are interested in, e.g. the deep-water replacement current in the Strait of Georgia (LeBlond *et al.* 1991; Karsten *et al.* 1995) has $\mu \simeq 1$.

The upper-layer dynamic density field and vertical and horizontal velocities, lower-layer horizontal velocity and geostrophic pressure are determined, respectively, by

$$\rho = -\varphi_z, \tag{1.5}$$

$$w = -N^{-2}[\varphi_{zt} + \mu J(\varphi, \varphi_z)], \tag{1.6}$$

$$\boldsymbol{u}_1 = \boldsymbol{e}_3 \times \nabla\varphi, \tag{1.7}$$

$$\boldsymbol{u}_2 = \boldsymbol{e}_3 \times \nabla[h_{\mathrm{B}} + \mu(\varphi\,|_{z=-1} + h)], \tag{1.8}$$

$$p = h_{\mathrm{B}} + \mu(\varphi\,|_{z=-1} + h), \tag{1.9}$$

where the Jacobian is given by $J(A, B) = A_x B_y - A_y B_x$, $\nabla = (\partial_x, \partial_y)$ and $\Delta = \nabla^2$. Alphabetical subscripts indicate partial differentiation unless otherwise indicated, and the subscript 1 or 2 refers to the upper or lower layers, respectively. Note that the lower-layer geostrophic pressure, given by (1.9), is not simply the lower-layer height, and that it is strongly coupled to the upper layer. Equations (1.1)–(1.4) are just the quasi-geostrophic equations for a continuously stratified fluid where the usual lower boundary condition is replaced by (1.3) and (1.4), which couples the evolution of lower-layer height to the upper-layer geostrophic pressure.

The lower-layer equation (1.4) can be thought of as the mass-conservation equation for a geostrophically balanced flow as determined by (1.8). Alternatively, (1.4) can be thought of as the leading-order potential vorticity equation for the lower layer under a planetary geostrophic approximation (Pedlosky 1984) scaled for shelf dynamics, where the background vorticity gradient is provided by the sloping topography. In this connection, it is worthwhile noting that the instability problem associated

with our model does not suffer from an ultraviolet catastrophe like most planetary geostrophic models (see part I and de Verdiere 1986).

2. General remarks and a variational principle

For the purposes of this paper, we henceforth assume the constant slope-bottom topography $h_B = -y$, and take the horizontal domain as $\mathbb{R}^2$. Thus, the coordinate system has x and y oriented in the along- and cross-slope directions, respectively (see figure 1). In this section, we examine arbitrary nonlinear steadily travelling solutions to the model.

Let us consider solutions to (1.1)–(1.4), which can be written in terms of the co-moving variables

$$\xi = x - ct, \qquad \zeta = y - \tilde{c}t, \tag{2.1}$$

where c and $\tilde{c}$ are the along- and cross-slope velocities, respectively. Substitution of (2.1) and

$$(\varphi, h) = (\varphi_s(\xi, \zeta), h_s(\xi, \zeta)),$$

where the subscript 's' denotes the steadily travelling ansatz, into the governing equations leads to

$$J(\mu\varphi_s + c\zeta - \tilde{c}\xi, \Delta\varphi_s + (N^{-2}\varphi_{s_z})_z) = 0, \tag{2.2}$$

$$J(\mu\varphi_s + c\zeta - \tilde{c}\xi, \varphi_{s_z}) = 0, \qquad \text{on } z = 0, \tag{2.3}$$

$$J(\mu\varphi_s + c\zeta - \tilde{c}\xi, \varphi_{s_z} + N^2(h_s - \zeta/\mu)) = \tilde{c}N^2/\mu, \quad \text{on } z = -1, \tag{2.4}$$

$$J(\mu\varphi_s + (c-1)\zeta - \tilde{c}\xi, h_s) = 0, \qquad \text{on } z = -1. \tag{2.5}$$

In general, the coupling between the two layers leads to both along- and cross-slope motion. If we compute the ξ and ζ moments of (2.5), we obtain, respectively,

$$c = 1 - \mu \frac{\displaystyle\iint_{\mathbb{R}^2} h_s \varphi_{s_\zeta}\,|_{z=-1}\ \mathrm{d}\xi\mathrm{d}\zeta}{\displaystyle\iint_{\mathbb{R}} h_s\,\mathrm{d}\xi\mathrm{d}\zeta}, \tag{2.6}$$

$$\tilde{c} = \mu \frac{\displaystyle\iint_{\mathbb{R}} h_s \varphi_{s_\xi}\,|_{z=-1}\ \mathrm{d}\xi\mathrm{d}\zeta}{\displaystyle\iint_{\mathbb{R}} h_s\,\mathrm{d}\xi\mathrm{d}\zeta}. \tag{2.7}$$

These are the continuously stratified analogues of the two-layer translation velocities derived by Swaters & Flierl (1991). Note that in the non-interacting limit $\mu \to 0$, it follows that $(c, \tilde{c}) = (1, 0)$, which recovers the Nof (1983) result.

However, if there are closed streak lines, that is, simply connected isolines of the co-moving stream function given by

$$\psi_{\text{streak lines}} = \mu\varphi_s + c\zeta - \tilde{c}\xi,$$

then it follows that $\tilde{c}N^2(-1) = 0$. The argument is similar to that presented by Flierl *et al.* (1980) disallowing meridional motion for non-radiating β-plane modons.

Consider a finite region $A \subset \mathbb{R}^2$ the boundary of which, denoted as ∂A, corresponds to a streak line. If (2.4) is integrated over A, it follows that

$$\frac{\tilde{c}N^2(-1)\|A\|}{\mu} = \iint_A [J(\mu\varphi_s + c\zeta - \tilde{c}\xi, \varphi_{s_z} + N^2(h_s - \zeta/\mu))]_{z=-1}\,\mathrm{d}\xi\mathrm{d}\zeta$$
$$= \int_{\partial A} [\boldsymbol{n} \times \nabla(\mu\varphi_s + c\zeta - \tilde{c}\xi)(\varphi_{s_z} + N^2(h_s - \zeta/\mu))]_{z=-1}\,\mathrm{d}s = 0, \quad (2.8)$$

since

$$[\boldsymbol{n} \times \nabla(\mu\varphi_s + c\zeta - \tilde{c}\xi)]_{\partial A} = 0,$$

where $\|A\|$ denotes the area of A, and where $\mathrm{d}s$ is the differential arclength. Thus, we conclude that $\tilde{c}N^2(-1) = 0$ if there are closed streak lines, which, for general stratification, implies that $\tilde{c} = 0$, i.e. there cannot be any cross-slope motion.

Assuming that $\tilde{c} = 0$ allows (2.2)–(2.5) to be integrated in the form

$$\mu\varphi_s + c\zeta = F_1(\Delta\varphi_s + (N^{-2}\varphi_{s_z})_z), \quad (2.9)$$
$$\mu\varphi_s + c\zeta = F_2(\varphi_{s_z}), \quad \text{on } z = 0, \quad (2.10)$$
$$\mu\varphi_s + c\zeta = F_3(\varphi_{s_z} + N^2(h_s - \zeta/\mu)), \quad \text{on } z = -1, \quad (2.11)$$
$$\mu\varphi_s + (c-1)\zeta = F_4(h_s), \quad \text{on } z = -1, \quad (2.12)$$

where F_1, F_2, F_3 and F_4 are arbitrary functions of their arguments.

In general, one needs to know the detailed structure of h_s and φ_s to determine the F_i functions. However, if the eddy is isolated (i.e. both h_s and $\varphi_s \to 0$ at infinity), then it follows from (2.11) that

$$F_3(*) = -\frac{c\mu}{N^2(-1)}*,$$

so that (2.11) reduces to

$$\varphi_{s_z} + [N^2/c]\varphi_s = -N^2 h_s, \quad \text{on } z = -1, \quad (2.13)$$

for all those streak lines on $z = -1$ that extend to infinity.

For those streak lines on $z = -1$ that do not extend to infinity (i.e. a region of closed streak lines), the above argument does not formally hold. In principle, one is left free to specify an entirely different form for F_3, e.g. a non-analytic function similar to that which holds for the modon (Larichev & Reznik 1976; Flierl *et al.* 1980). Here, however, we follow, for example, Hogg (1980) or Swaters & Mysak (1985) in their treatment of nonlinear eddies in a continuously stratified fluid and apply (2.13) throughout the domain. This is perhaps the simplest choice that will ensure that the stream function and vorticity in the upper fluid will be smooth across the boundary separating the regions of closed and open streak lines.

It is possible to obtain a variational principle for the eddies described by (2.9)–(2.12). First, observe that for $h_B = -y$ and the horizontal domain given by $\mathbb{R}^2$, the Hamiltonian structure (see part I, § 2) for (1.1)–(1.4) is invariant to arbitrary translations with respect to x. Consequently, by Noether's theorem (see, for example, Benjamin 1984; Shepherd 1990), the x-direction impulse functional, denoted by $\mathcal{I}$, and determined by solving

$$\mathcal{M}\frac{\delta\mathcal{I}}{\delta\boldsymbol{q}} = -\boldsymbol{q}_x,$$

where $\mathcal{M}$ and $\boldsymbol{q} = (q_1, q_2, q_3, q_4)^{\mathrm{T}}$ are, respectively, the cosymplectic form and Hamiltonian variables given by equations (2.12), (2.13) and (2.15) in part I, is an invariant of the dynamics.

It is straightforward to verify that

$$\mathcal{I} = \iiint_{\Omega} y\Delta\varphi \,\mathrm{d}x\mathrm{d}y\mathrm{d}z, \tag{2.14}$$

and that the relations (2.9)–(2.12) satisfy the first-order necessary conditions for an extremal of the conserved (constrained energy) functional

$$\hat{H}(\boldsymbol{q}) = H - c\mathcal{I} + C, \tag{2.15}$$

i.e.

$$\delta\hat{H}(\boldsymbol{q}_{\mathrm{s}}) = 0,$$

where the Hamiltonian H can be written in the form

$$H = \tfrac{1}{2}\mu \iiint_{\Omega} \nabla\varphi\cdot\nabla\varphi + (\varphi_z/N)^2 \,\mathrm{d}x\mathrm{d}y\mathrm{d}z + \tfrac{1}{2}\mu \iint_{\mathbb{R}^2} (h + h_{\mathrm{B}}/\mu)^2 - (h_{\mathrm{B}}/\mu)^2 \,\mathrm{d}x\mathrm{d}y, \tag{2.16}$$

where the three-dimensional spatial domain is given by

$$\Omega = \mathbb{R}^2 \times (-1, 0),$$

and the Casimir functional C is given by

$$C = \iiint_{\Omega} \Phi_1(q_1) \,\mathrm{d}x\mathrm{d}y\mathrm{d}z + \iint_{\mathbb{R}^2} \Phi_2(q_2) + \Phi_3(q_3) + \Phi_4(q_4) \,\mathrm{d}x\mathrm{d}y, \tag{2.17}$$

with the density functions

$$\left.\begin{aligned} \Phi_1(q_1) &= \int_0^{q_1} F_1(\tau)\,\mathrm{d}\tau, \\ \Phi_2(q_2) &= -N^{-2}(0)\int_0^{q_2} F_2(\tau)\,\mathrm{d}\tau, \\ \Phi_3(q_3) &= N^{-2}(-1)\int_{-N^2(-1)y/\mu}^{q_3} F_3(\tau)\,\mathrm{d}\tau, \\ \Phi_4(q_4) &= -\tfrac{1}{2}\mu q_4^2 - \int_0^{q_4} F_4(\tau)\,\mathrm{d}\tau, \end{aligned}\right\} \tag{2.18}$$

and where

$$\left.\begin{aligned} q_1 &= \Delta\varphi + (N^{-2}\varphi_z)_z, \\ q_2 &= \varphi_z\,|_{z=0}, \\ q_3 &= \varphi_z\,|_{z=-1} + N^2(-1)(h + h_{\mathrm{B}}/\mu), \\ q_4 &= h. \end{aligned}\right\} \tag{2.19}$$

Unfortunately, even though $\delta\hat{H}(\boldsymbol{q}_{\mathrm{s}}) = 0$, it can be viewed as a consequence of Andrews's theorem (Andrews 1984), that one cannot use $\hat{H}$ to establish Arnol'd-like stability theorems for isolated steadily travelling eddies (similar to those obtained in part I for steady solutions). The only isolated flows that can satisfy the stability conditions ensuring that $\delta^2\hat{H}(\boldsymbol{q}_{\mathrm{s}})$ is definite are those for which $\varphi_{\mathrm{s}_x} = h_{\mathrm{s}_x} \equiv 0$ everywhere. For isolated eddies we require $|\varphi_{\mathrm{s}}, h_{\mathrm{s}}| \to 0$ as $x^2 + y^2 \to \infty$, which will imply that only the trivial solution can satisfy the conditions for Arnol'd stability. Full details of the argument can be found in Poulin (1997).

3. Radially symmetric isolated eddies

Let us assume, again, that $h_{\mathrm{B}} = -y$, and consider steadily travelling solutions of the form

$$h = h(r), \qquad \varphi = \varphi(r, z), \qquad r = \sqrt{\xi^2 + y^2}, \tag{3.1}$$

where $\xi = x - ct$. From (2.6) it follows that $c = 1$, since the $O(\mu)$ term is identically zero. Substitution of (3.1) into (2.2)–(2.5), with $\tilde{c} = 0$, leads to

$$r^{-1}(r\varphi_r)_r + (N^{-2}\varphi_z)_z = 0, \tag{3.2}$$

$$\varphi_z = 0, \qquad \text{on } z = 0, \tag{3.3}$$

$$\varphi_z + N^2\varphi = -N^2 h, \quad \text{on } z = -1. \tag{3.4}$$

Thus, given a cold pool height profile $h(r)$, we determine $\varphi(r, z)$ by solving (3.2)–(3.4).

The first thing to note is that this boundary-value problem is neither separable nor Sturm–Liouville. This implies that the eigenvalues of the operator $r^{-1}(r\partial_r)_r + (N^{-2}\partial_z)_z$ are not all negative, that is, there will be a finite number of positive eigenvalues. The horizontal field associated with the positive eigenvalues can be written in terms of *ordinary* Bessel functions. However, since ordinary Bessel functions decay like $O(r^{-1/2})$ as $r \to \infty$, it follows that to have finite-energy solutions one has to impose a zero wave constraint similar to the two-layer solutions obtained by Swaters & Flierl (1991). The horizontal field associated with the negative eigenvalues can be written in terms of *modified* Bessel functions that decay exponentially rapidly for large r and so do not give rise to any wave field in the far field.

Another point to make is that *all* finite-energy/mass solutions to (3.2)–(3.4) will satisfy the continuously stratified analogue of the *Mory–Stern isolation constraint* (Mory 1985; Mory *et al.* 1987) for our model. If we integrate (3.2) over Ω, it follows that

$$\begin{aligned}\iiint_{\Omega} r^{-1}(r\varphi_r)_r + (N^{-2}\varphi_z)_z r \,\mathrm{d}r\mathrm{d}\theta\mathrm{d}z &= -\iint_{\mathbb{R}^2} N^{-2}\varphi_z \mid_{z=-1} r \,\mathrm{d}r\mathrm{d}\theta \\ &= \iint_{\mathbb{R}^2} h + \varphi \mid_{z=-1} r \,\mathrm{d}r\mathrm{d}\theta = 0,\end{aligned} \tag{3.5}$$

where we have integrated by parts using (3.3) and (3.4) and the fact that $\boldsymbol{n}\cdot\nabla\varphi \to 0$ as $r \to \infty$. Thus, there must be a negative pressure anomaly in the upper layer to compensate for positive h.

As in the isolated eddy solutions found by Swaters & Flierl (1991), the solutions found here will possess the property that the swirl velocity, denoted as v_{swirl}, in the lower layer (i.e. the azimuthal velocity in the translating frame of reference) will not be solely anticyclonic. We may write (3.5) in the form

$$\begin{aligned}-2\iint_{\mathbb{R}^2} h + \varphi \mid_{z=-1} r \,\mathrm{d}r\mathrm{d}\theta &= \iint_{\mathbb{R}^2} r^2(h + \varphi \mid_{z=-1})_r \,\mathrm{d}r\mathrm{d}\theta \\ &= \frac{1}{\mu}\iint_{\mathbb{R}^2} r^2 v_{\mathrm{swirl}} \,\mathrm{d}r\mathrm{d}\theta = 0,\end{aligned} \tag{3.6}$$

where (1.8) and (1.9) have been used. Thus, we see that v_{swirl} must take on positive as well as negative values for the Mory–Stern isolation constraint to hold.

In practice, we have found that v_{swirl} is mostly negative with a band of cyclonic circulation near the eddy boundary. We will illustrate this point with an exact solution presented later in the section. We note, however, that we have not been able to discern this structure in any of the experiments described in the literature (see, for example, Mory *et al.* 1987; Honji & Hosoyamada 1989; Whitehead *et al.* 1990). This is an interesting prediction of our theory and it would be valuable to check whether or not this property can be observed in an experiment or oceanographic data.

We complete this subsection by solving (3.2)–(3.4) assuming, for simplicity, constant stratification. Consider the eigenvalue problem

$$N^{-2}\Phi_{zz} = \lambda\Phi, \tag{3.7}$$

$$\Phi_z = 0, \qquad \text{on } z = 0, \tag{3.8}$$

$$\Phi_z + N^2\Phi = 0, \qquad \text{on } z = -1. \tag{3.9}$$

It is straightforward to verify that there is only a single positive eigenvalue and that all the rest are negative. The orthonormal eigenfunctions are denoted as the set $\{\lambda_n, \Phi_n(z)\}_{n=0}^{\infty}$, and are given by

$$\Phi_0(z) = \left[\frac{2(\lambda_0 - N^2)}{\lambda_0 + 1 - N^2}\right]^{1/2} \cosh(\sqrt{\lambda_0}Nz),$$

$$\Phi_n(z) = \left[\frac{2(N^2 - \lambda_n)}{N^2 + 1 - \lambda_n}\right]^{1/2} \cos(\sqrt{-\lambda_n}Nz),$$

for $n = 1, 2, \ldots$, where

$$\tanh(\sqrt{\lambda_0}N) = \frac{N}{\sqrt{\lambda_0}},$$

$$\tan(\sqrt{-\lambda_n}N) = -\frac{N}{\sqrt{-\lambda_n}}, \quad \text{for } n = 1, 2, \ldots,$$

and where

$$\int_{-1}^{0} \Phi_n(z)\Phi_m(z)\,\mathrm{d}z = \delta_{nm}.$$

The solution to (3.2)–(3.4) may be constructed in the form

$$\varphi(r, z) = \sum_{n=0}^{\infty} A_n(r)\Phi_n(z). \tag{3.10}$$

To obtain the governing equation for $A_n(r)$ we multiply (3.2) by $\Phi_n(r)$ and integrate with respect to z and exploit the boundary conditions, yielding

$$\left(r\frac{\mathrm{d}^2}{\mathrm{d}r^2} + \frac{\mathrm{d}}{\mathrm{d}r} + r\lambda_n\right)A_n = -\Phi_n(-1)rh, \quad \text{for } n = 0, 1, 2, \ldots. \tag{3.11}$$

We assume that h is a continuous function of compact support of the form

$$h = \begin{cases} h(r), & \text{for } 0 \leqslant r < a, \\ 0, & \text{for } r \geqslant a, \end{cases} \tag{3.12}$$

with $h(a) = 0$. Thus, the solution for A_0 that is bounded at the origin is given by

$$A_0(r) = -\frac{\pi\Phi_0(-1)}{2}\left\{Y_0(\sqrt{\lambda_0}r)\int_0^r \varsigma J_0(\sqrt{\lambda_0}\varsigma)h(\varsigma)\,\mathrm{d}\varsigma + J_0(\sqrt{\lambda_0}r)\int_r^a \varsigma Y_0(\sqrt{\lambda_0}\varsigma)h(\varsigma)\,\mathrm{d}\varsigma\right\}. \quad (3.13)$$

To remove the wave field ahead of the propagating eddy, we require

$$\int_0^a \varsigma J_0(\sqrt{\lambda_0}\varsigma)h(\varsigma)\,\mathrm{d}\varsigma = 0, \quad (3.14)$$

which is identical to the zero wave constraint found in Swaters & Flierl (1991) and is equivalent to the Mory–Stern isolation constraint (3.5). Thus, $A_0(r)$ is given by (3.13) for $0 \leqslant r < a$ and $A_0(r) \equiv 0$ for $r \geqslant a$. We note that (3.14) ensures that $A_0(r)$ is continuously differentiable at $r = a$ so that $A_{0_r}(a) = 0$.

The solutions for $\{A_n\}_{n=1}^{\infty}$ that are bounded at the origin, and which decay exponentially rapidly at infinity, are given by

$$A_n(r) = \Phi_n(-1)\left\{K_0(\sqrt{-\lambda_n}r)\int_0^r \varsigma I_0(\sqrt{-\lambda_n}\varsigma)h(\varsigma)\,\mathrm{d}\varsigma + I_0(\sqrt{-\lambda_n}r)\int_r^a \varsigma K_0(\sqrt{-\lambda_n}\varsigma)h(\varsigma)\,\mathrm{d}\varsigma\right\}, \quad \text{for } 0 \leqslant r < a, \quad (3.15)$$

and

$$A_n(r) = \Phi_n(-1)K_0(\sqrt{-\lambda_n}r)\int_0^a \varsigma I_0(\sqrt{-\lambda_n}\varsigma)h(\varsigma)\,\mathrm{d}\varsigma, \quad \text{for } r \geqslant a. \quad (3.16)$$

These solutions do not have a wave field ahead of the propagating eddy. The solutions for $\{A_n(r)\}_{n=0}^{\infty}$ will *all* possess finite area-integrated energy and enstrophy as required, and be continuously differentiable everywhere.

Only if μ is sufficiently large will there be closed streak lines, that is, fluid parcels in the upper layer that will be transported by the steadily travelling eddy. The critical μ—denoted μ_c, for which any $\mu > \mu_c$ will imply that there are closed streak lines—is the first value of μ for which a stagnation point first develops in the co-moving frame, i.e. the first μ for which

$$\nabla(\mu\varphi + y) = \mathbf{0}, \quad (3.17)$$

somewhere in the flow (Huppert 1975).

(*a*) *A parabolic eddy example*

In order to illustrate the vertical and horizontal structure of these eddies, let us consider the very simple example

$$h = \begin{cases} 1 - (r/a)^2, & \text{for } 0 \leqslant r < a, \\ 0, & \text{for } r \geqslant a. \end{cases} \quad (3.18)$$

The gravest mode Fourier coefficient A_0 is given by

$$A_0(r) = \frac{4\Phi_0(-1)}{a^2\lambda_0^2}\left[\frac{J_0(\sqrt{\lambda_0}r)}{J_0(\sqrt{\lambda_0}a)} - 1\right] - \frac{\Phi_0(-1)}{\lambda_0}\left[1 - \left(\frac{r}{a}\right)^2\right], \quad (3.19)$$

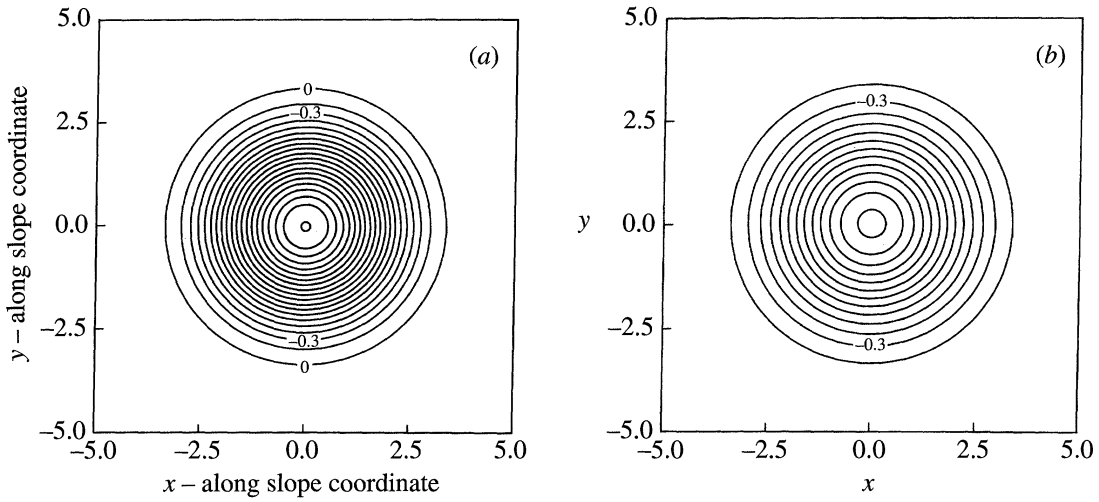

Figure 2. Contour plots of the upper-layer stream function or geostrophic pressure for an isolated eddy at (*a*) $z = -1.0$, and (*b*) $z = 0.0$. The pressure anomaly is negative and the contour interval is 0.15.

and the isolation constraint (3.14) reduces to

$$J_2(\sqrt{\lambda_0}a) = 0. \tag{3.20}$$

We may write the $\{A_n\}_{n=1}^{\infty}$ solutions in the form

$$A_n(r) = \Gamma_{1,n} I_0(\sqrt{-\lambda_n}r) - \frac{4\Phi_n(-1)}{a^2\lambda_n^2} - \frac{\Phi_n(-1)}{\lambda_n}\left[1 - \left(\frac{r}{a}\right)^2\right], \tag{3.21}$$

for $0 \leqslant r < a$, and

$$A_n(r) = \Gamma_{2,n} K_0(\sqrt{-\lambda_n}r), \quad \text{for } r \geqslant a, \tag{3.22}$$

where $\Gamma_{1,n}$ and $\Gamma_{2,n}$ are given, respectively, by

$$\Gamma_{1,n} = -\frac{2\Phi_n(-1)K_2(\sqrt{-\lambda_n}a)}{\lambda_n}, \tag{3.23}$$

$$\Gamma_{2,n} = -\frac{2\Phi_n(-1)I_2(\sqrt{-\lambda_n}a)}{\lambda_n}. \tag{3.24}$$

In order to illustrate the spatial characteristics of the solution, we set $N = \mu = 1.0$ initially. We find that the first four vertical eigenvalues are given by, approximately, $\lambda_0 = 1.44$, $\lambda_1 = -7.83$, $\lambda_2 = -37.47$ and $\lambda_3 = -86.82$, respectively. In practice, we found that the spatial structure was very well described by retaining only the first four vertical modes. We take the so-called ground state value for the radius, i.e. the first non-zero solution to (3.20), which implies that, approximately, $a = 4.28$.

In figure 2*a*, *b* we show horizontal contour plots of the upper-layer stream function or geostrophic pressure at $z = -1.0$ and 0.0, respectively, i.e. immediately over the cold dome and on the surface, respectively. The contour interval is 0.15. The along-slope direction corresponds to left to right in the panels, and bottom to top corresponds to the direction of increasing water depth. The eddy travels from left to right in the panels.

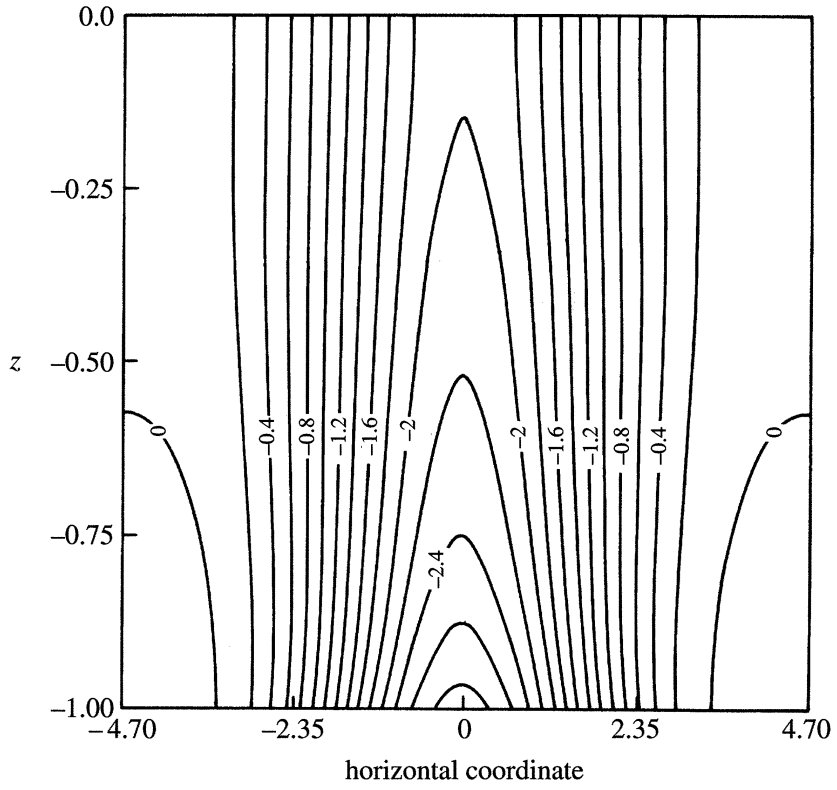

Figure 3. Vertical cross-section through the eddy centre of the upper-layer geostrophic pressure. The contour interval is 0.2.

In the upper layer, the eddy corresponds to a negative pressure anomaly that leads to cyclonic circulation. The boundary of the eddy is the 0-contour. The eddy extends vertically throughout the water column, but is bottom intensified. One can see this in figure $2a, b$, in that there are more contours in the $z = -1.0$ panel than in the $z = 0.0$ panel (both have the same contour interval).

The full vertical structure can be inferred from figure 3, which depicts a vertical cross-section through the eddy centre of the upper-layer geostrophic pressure. The contour interval is 0.2. The minimum pressure anomaly occurs at the bottom with a non-dimensional value a little less than -2.8. The pressure monotonically increases upward and radially outward. The eddy boundary is located at the 0-contour.

In figure 4 we show a contour plot of the 'swirl pressure' within the eddy interior. The swirl pressure is the geostrophic pressure associated with the azimuthal velocity in the co-moving frame of reference, i.e. $\mu(\varphi + h)$. The contour interval is 0.1. There is an interior region near the centre where the swirl pressure is negative, and an outer region beside the eddy boundary where the swirl pressure is positive. Note that there are two 0-contours. The radially outward one is the eddy boundary and the interior one separates the negative and positive swirl-pressure regions.

The swirl pressure is maximum just radially inward of the eddy boundary. The annular region bounded radially inward by the contour associated with the maximum swirl pressure, and radially outward by the eddy boundary, has the property that

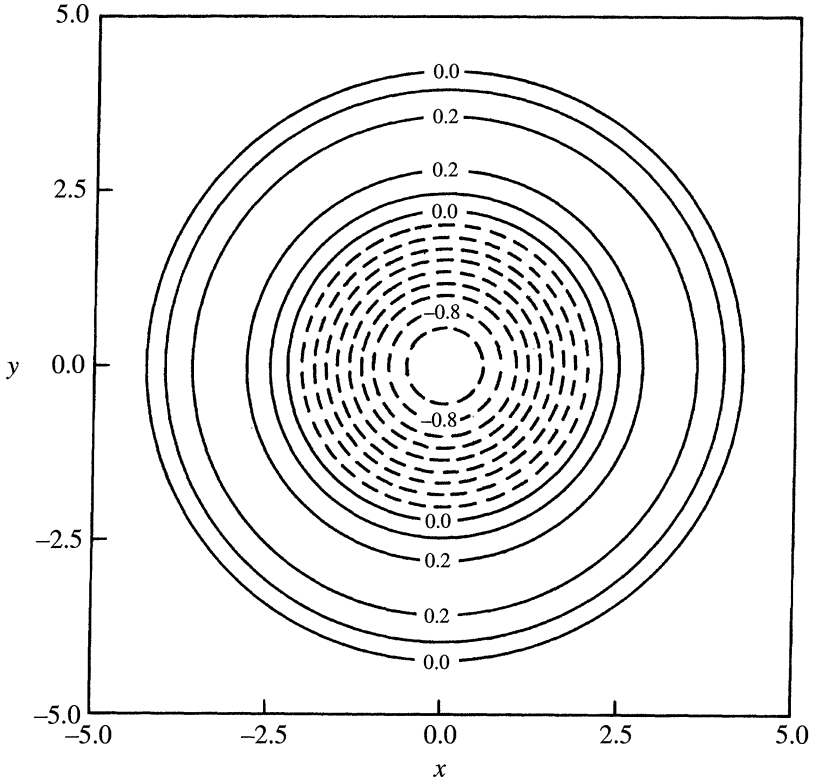

Figure 4. Contour plot of the 'swirl pressure' in the eddy interior. The contour interval is 0.1.

$(\varphi + h)_r < 0$. In this region, the swirl velocity will be positive, i.e. cyclonic flow. In the core of the eddy, which is bounded radially outward by the contour associated with the maximum swirl pressure, it follows that $(\varphi + h)_r > 0$. In this region, the swirl velocity will be negative, i.e. anticyclonic flow. Thus, while the circulation in the interior of the eddy is for the most part anticyclonic, there is a band of cyclonic circulation located near the eddy boundary as required in order to satisfy the Mory–Stern isolation constraint (3.5) and its consequence (3.6).

For this value of the interaction parameter (i.e. $\mu = 1$), the eddy does not transport fluid parcels throughout the entire upper-layer water column. In figure 5*a*, *b* we show a contour plot of the streak lines, i.e. the upper-layer stream function in the co-moving frame, given by $\mu\varphi + y$ for $z = -1.0$ and $z = 0.0$, respectively. The contour interval is 0.4. In figure 5*a* we see that there is a small region of closed streak lines. Those fluid parcels in this region will be transported by the eddy. As it turns out, however, this region is confined to the near-bottom region. For virtually all the water column, upper-layer fluid parcels are not transported by the eddy. In figure 5*b* we show the streak lines on the surface $z = 0.0$. There are no closed streak lines.

It does not take a large value of the interaction parameter for a vertically extended region of closed streak lines to develop. In figure 6*a*, *b* we show contour plots of the streak lines assuming $\mu = 2.0$ for $z = -1.0$ and 0.0, respectively. The contour interval is 0.4, which is the same as that in figure 5. One can see the enhanced region of closed contours at $z = -1.0$. For this value of μ the region of closed streak lines extends

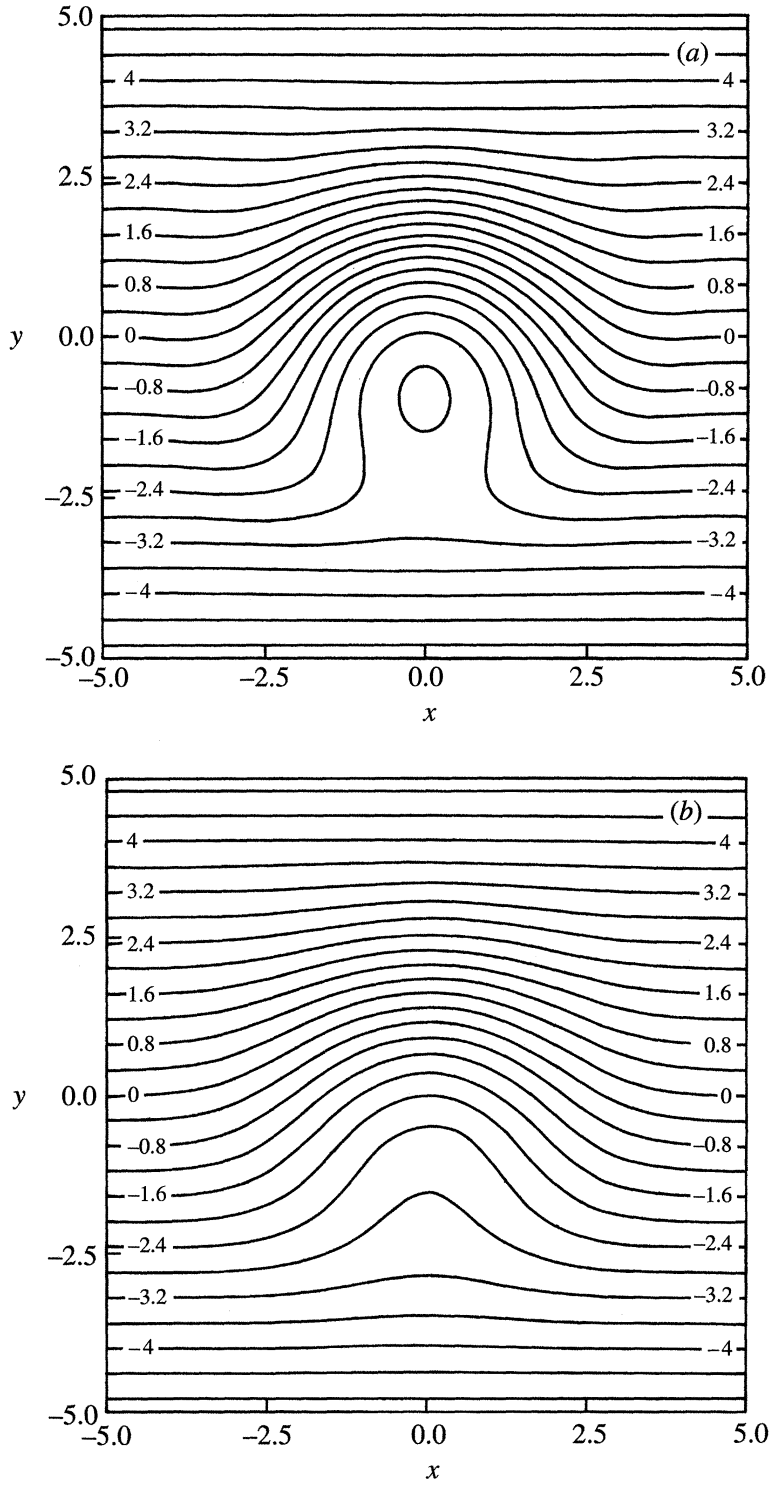

Figure 5. Contour plots of the upper-layer streak lines for an isolated eddy with $\mu = 1.0$ at (*a*) $z = -1.0$ and (*b*) $z = 0.0$. The contour interval is 0.4.

throughout the water column. One can clearly see a region of closed streak lines on the surface $z = 0.0$.

These values of μ are quite reasonable. Swaters & Flierl (1991) estimated that $\mu \approx 2.0$ for the cold pool observed on the New England Bight (Houghton *et al.* 1982). Karsten *et al.* (1985) estimated that $\mu \approx 1.0$ for the deep-water replacement current in the strait of Georgia (LeBlond *et al.* 1991). We therefore conclude that for realistic values of the interaction parameter, the cyclonic eddies generated in the overlying fluid, are able to transport intermediate and near-surface waters.

4. Radiating cold-dome solutions

It is unlikely that observed density-driven baroclinic eddies would be isolated, that is, one expects that a topographic Rossby wave field would be generated in the upper fluid. It is, therefore, of interest to determine the effect that an upper-layer topographic wave field has on the propagation characteristics of the eddy solutions of the model. Unfortunately, we have not been able to construct an exact solution for a fully nonlinear coupled eddy-topographic Rossby wave configuration.

However, much can be learned from examining the weakly interacting, i.e. small-μ, limit of the governing equations (1.1)–(1.4). Specifically, we can construct an exact, to leading order, coupled eddy-topographic Rossby wave solution, which satisfies the appropriate radiation condition ahead of the travelling eddy, and explicitly compute the along- and cross-slope velocities. The external Rossby wave field radiates energy away from the eddy interior, but this is a higher-order effect (see, for example, Flierl 1984). To be asymptotically consistent with the expansion used in deriving (1.1)–(1.4), it is formally assumed that $0 < s \ll \mu \ll 1$.

The parameter μ can be written as (see § 1 *a* and part I)

$$\mu = h_*/(s^* L),$$

where $L = \sqrt{g'\overline{H}}/f$ is the horizontal length-scale. A small-μ assumption can be thought of as either a 'thin' lower layer, 'long' horizontal length-scale, or a 'steep' slope approximation (within the underlying modelling scalings described in part I).

A word of caution is appropriate here. Oceanographically relevant estimates of μ suggest that it is an $O(1)$ parameter and *not* small (see, for example, Swaters & Flierl 1991; Karsten *et al.* 1995). However, we believe that much can be learned from the solution we obtain here about the structure of a radiating baroclinic cold dome, even if the underlying expansion is somewhat more formal than we would like.

In addition, we note as a pool of cold, dense, homogeneous fluid intrudes into a stratified fluid it will, of course, modify the ambient stratification, which will, in turn, affect the coupled dynamics between the cold pool and the surrounding fluid. Although there appears to be no oceanographic data explicitly describing the evolution of the overlying stratification associated with these propagating mesoscale cold domes, Houghton *et al.* (1982) did describe the along-shelf evolution of the temperature field associated with a cold dome that formed on the New England Bight. The observations showed a warming of the cold dome of *ca.* 2 °C per month. That is, the density contrast between the cold dome and the surrounding fluid diminished over time.

Swaters & Flierl (1991) examined this effect using a two-layer analogue of the present model, which incorporated a simple 'mixing' term in which colder dome

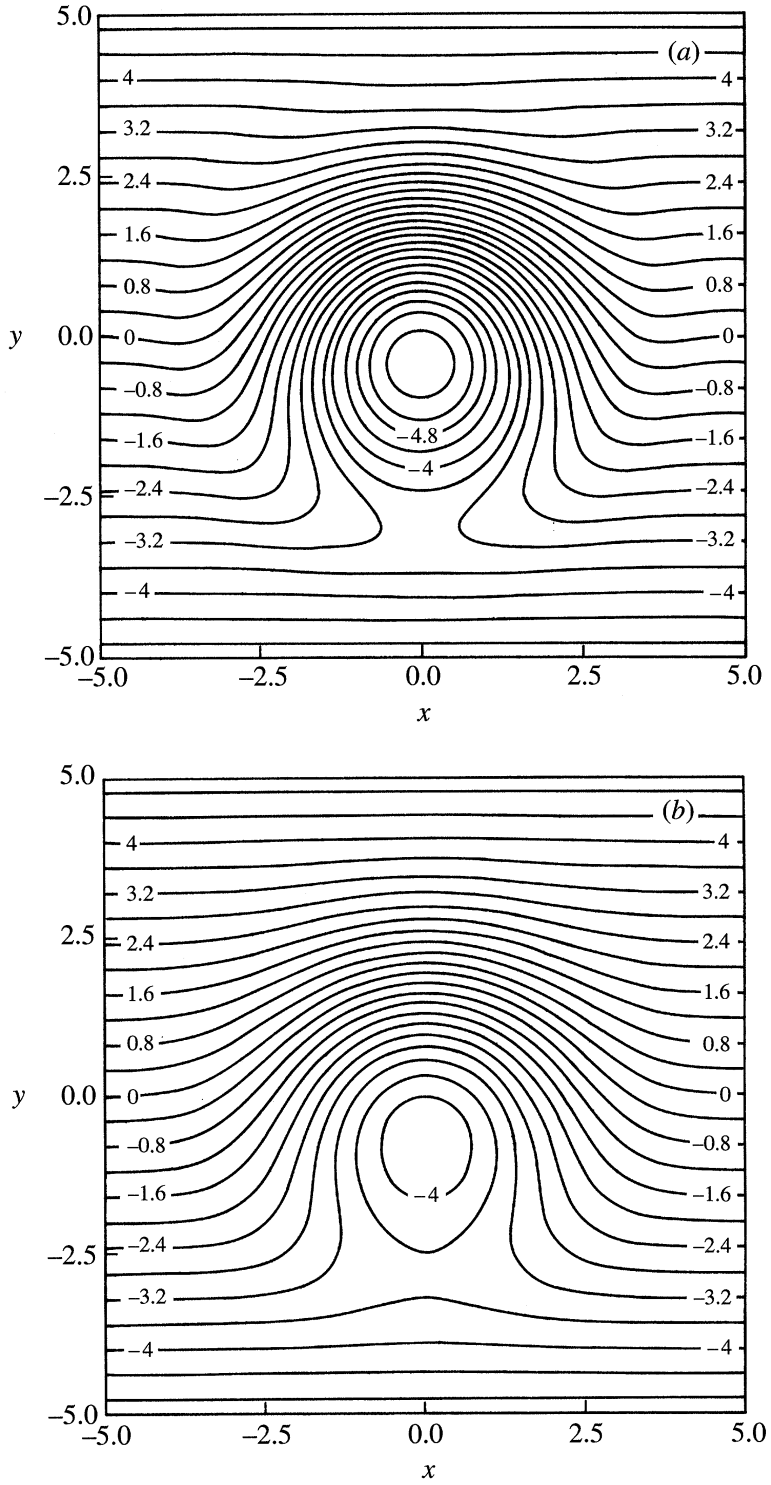

Figure 6. Contour plots of the upper-layer streak lines for an isolated eddy with $\mu = 2.0$ at (*a*) $z = -1.0$ and (*b*) $z = 0.0$. The contour interval is 0.4.

water was continuously converted into upper-layer water (within total mass conservation). Swaters & Flierl (1991) showed that this mixing resulted in the *up-slope* motion of the cold dome. The up-slope motion is a consequence of potential vorticity conservation in the upper layer, in that as the cold dome diminishes in height due to mass conversion, this results in a decrease in the upper-layer potential vorticity, which is compensated for (since the potential vorticity is conserved to leading order) by the up-slope motion of the cold dome, which corresponds to moving to a position with increased background potential vorticity (moving up slope is like moving northward on a planetary β-plane).

The direction of cross-slope motion induced by the topographic Rossby wave field is *completely opposite*. As we show below, the effect of the topographic Rossby wave field will be to induce *down-slope* motion. This occurs because the energy source for the wave field will be the potential energy associated with the cross-slope position of the cold dome. As energy is radiated away by the topographic Rossby wave field, the cold dome slides down the slope, releasing its available potential energy.

While there has been no definitive study determining which effect is dominant, Mory *et al.* (1987), based on rotating-tank laboratory experiments of cold domes, thought they saw evidence of a trailing topographic wave field and did not report any induced changes to the ambient stratification. This may be a result of the fact that for the scales of motion involved, there is little excitation of very-small-scale internal gravity waves, which would be the mechanism by which the overlying stratification would change. As is well known in the theory of stratified flow over an obstacle (see, for example, Baines 1995, § 5.2), if $N^*a/U \gg 1$, where N^*, a and U are the Brunt–Väisälä frequency, half-width of the obstacle, and scale flow velocity, respectively, the flow is in hydrostatic balance, and the only part of the internal wavenumber spectrum that has meaningful energy corresponds to those wavelengths satisfying $\lambda \gg 2\pi U/N^*$. For the cold domes we are interested in here, the radius is *ca.* $4 \times L \simeq 60\,\mathrm{km}$, $N^* \simeq 10^{-2}\,\mathrm{s}^{-1}$ and $U \simeq 4\,\mathrm{cm\,s}^{-1}$, which implies $N^*a/U \simeq 15\,000$ and $2\pi U/N^* \simeq 25\,\mathrm{m}$. These long internal gravity waves will not efficiently mix the stratification.

An alternative approach to this problem has recently been developed by Swaters (1998*b*). Swaters determined the propagation characteristics of a weakly radiating cold dome using the Swaters & Flierl (1991) two-layer model assuming an initial eddy that had a small, but non-zero, value associated with the integral in the Mory–Stern isolation constraint. Both approaches have their positive and negative features. The Swaters (1998*b*) approach allows for $O(1)$ values of μ, but requires an initial eddy radius near to that required to satisfy (3.14). The approach we present here does not require that (3.14) be 'almost' satisfied, but does require a small μ. As it turns out, both approaches will yield *identical* predictions for the leading-order cross-slope translation velocity.

It follows from (2.6) and (2.7) that the along- and cross-slope velocities are $O(1)$ and $O(\mu)$, respectively. Thus, if we introduce the co-moving coordinates

$$\xi = x - ct, \qquad \zeta = y - \mu\tilde{c}t, \tag{4.1}$$

into (1.1)–(1.4), and assume $h_{\mathrm{B}} = -y$, we obtain

$$c(\Delta\varphi + (N^{-2}\varphi_z)_z)_\xi = \mu J(\varphi - \tilde{c}\xi, \Delta\varphi + (N^{-2}\varphi_z)_z), \tag{4.2}$$

$$c\varphi_{z\xi} = \mu J(\varphi - \tilde{c}\xi, \varphi_z), \qquad \text{on } z = 0, \tag{4.3}$$

$$[c\varphi_z + N^2(\varphi + h)]_\xi = \mu[J(\varphi, \varphi_z) - \tilde{c}\varphi_{z\zeta}], \qquad \text{on } z = -1, \tag{4.4}$$

$$(c-1)h_\xi = \mu J(\varphi - \tilde{c}\xi, h), \qquad \text{on } z = -1. \tag{4.5}$$

The analogues of (2.6) and (2.7), which correspond to the ξ and ζ moments of (4.5), respectively, are given by

$$c = 1 - \mu \frac{\iint_{\mathbb{R}^2} h\varphi_\zeta \mid_{z=-1} \mathrm{d}\xi\mathrm{d}\zeta}{\iint_{\mathbb{R}^2} h \,\mathrm{d}\xi\mathrm{d}\zeta}, \tag{4.6}$$

$$\tilde{c} = \frac{\iint_{\mathbb{R}^2} h\varphi_\xi \mid_{z=-1} \mathrm{d}\xi\mathrm{d}\zeta}{\iint_{\mathbb{R}^2} h \,\mathrm{d}\xi\mathrm{d}\zeta}, \tag{4.7}$$

where it is understood that Δ and the Jacobian are now written with respect to ξ and ζ.

Introduction of the straightforward asymptotic expansion

$$(h, \varphi, c, \tilde{c}) \simeq (h, \varphi, c, \tilde{c})^{(0)} + \mu(h, \varphi, c, \tilde{c})^{(1)} + \cdots$$

into (4.2)–(4.5) leads to the $O(1)$ problem

$$\Delta\varphi^{(0)} + (N^{-2}\varphi_z^{(0)})_z = 0, \tag{4.8}$$

$$\varphi_z^{(0)} = 0, \qquad \text{on } z = 0, \tag{4.9}$$

$$\varphi_z^{(0)} + N^2\varphi^{(0)} = -N^2 h^{(0)}, \quad \text{on } z = -1, \tag{4.10}$$

with the translation velocities

$$c^{(0)} = 1, \tag{4.11}$$

$$c^{(1)} = -\frac{\iint_{\mathbb{R}^2} h^{(0)}\varphi_\zeta^{(0)} \mid_{z=-1} \mathrm{d}\xi\mathrm{d}\zeta}{\iint_{\mathbb{R}^2} h^{(0)} \,\mathrm{d}\xi\mathrm{d}\zeta}, \tag{4.12}$$

$$\tilde{c}^{(0)} = \frac{\iint_{\mathbb{R}^2} h^{(0)}\varphi_\xi^{(0)} \mid_{z=-1} \mathrm{d}\xi\mathrm{d}\zeta}{\iint_{\mathbb{R}^2} h^{(0)} \,\mathrm{d}\xi\mathrm{d}\zeta}. \tag{4.13}$$

In order to contrast this solution with the isolated radially symmetric solution previously described, we assume that $h^{(0)}$ is of the form (3.11), i.e.

$$h^{(0)} = \begin{cases} \tilde{h}(r), & \text{for } 0 \leqslant r < a, \\ 0, & \text{for } r \geqslant a, \end{cases} \tag{4.14}$$

with $\tilde{h}(a) = 0$. Since $c^{(0)}$ is positive and $\tilde{c}$ is $O(\mu)$, it follows that the appropriate 'no-upstream-waves' condition is, to leading order,

$$\varphi^{(0)} \simeq o(r^{-1/2}), \quad \text{as } r \to \infty \text{ in the sector } |\tan^{-1}(\zeta/\xi)| < \tfrac{1}{2}\pi. \tag{4.15}$$

To solve this boundary-value problem we proceed as in § 3. We assume a solution for $\varphi^{(0)}$ in the form (3.10) with $\Phi_n(z)$ given by (3.7)–(3.9). As before, the Fourier coefficients $A_n(r)$ will be the solutions of (3.11).

The gravest Fourier coefficient must solve

$$\left(r\frac{\mathrm{d}^2}{\mathrm{d}r^2}+\frac{\mathrm{d}}{\mathrm{d}r}+r\lambda_0\right)A_0=-\Phi_0(-1)rh^{(0)}, \tag{4.16}$$

subject to (4.15). A particular solution, denoted as $A_0^p(r)$, will be given by (3.13) for $0\leqslant r<a$, and by

$$-\tfrac{1}{2}\gamma\pi\Phi_0(-1)Y_0(\sqrt{\lambda_0}r), \tag{4.17}$$

where

$$\gamma=\int_0^a r\tilde{h}(r)J_0(\sqrt{\lambda_0}r)\,\mathrm{d}r, \tag{4.18}$$

for $a\leqslant r<\infty$. We assume that $\gamma\neq 0$, so that the particular solution has a topographic Rossby wave field associated with it, i.e. the zero wave condition (3.14) is *not* assumed to be satisfied.

In order to satisfy the no-upstream-waves condition (4.15), we must include a homogeneous solution to (4.16) of the form

$$\sum_{m=0}^{\infty}B_{2m+1}J_{2m+1}(\sqrt{\lambda_0}r)\cos[(2m+1)\theta], \tag{4.19}$$

where we are exploiting the radial symmetry and far-field asymptotic structure of (4.17) (see, for example, Flierl 1984; Swaters & Flierl 1991; Swaters 1998*b*). It follows that (4.15) will be satisfied provided

$$\tfrac{1}{2}\gamma\pi\Phi_0(-1)=\sum_{m=0}^{\infty}(-1)^mB_{2m+1}\cos[(2m+1)\theta], \tag{4.20}$$

in the sector $|\theta|<\frac{1}{2}\pi$. Consequently, we conclude that

$$B_{2m+1}=\frac{2\gamma\Phi_0(-1)}{2m+1}. \tag{4.21}$$

Thus, in summary, the solution for $A_0(r)$ can be written in the form

$$A_0(r)=A_0^p(r)+2\gamma\Phi_0(-1)\sum_{m=0}^{\infty}\frac{J_{2m+1}(\sqrt{\lambda_0}r)\cos[(2m+1)\theta]}{2m+1}, \tag{4.22}$$

where $A_0^p(r)$ is given by (3.13) for $0\leqslant r<a$ (with h replaced by $h^{(0)}$ given by (4.14)), and by (4.17) for $a\leqslant r<\infty$. This solution is continuously differentiable throughout $\mathbb{R}^2$.

The solutions for $\{A_n\}_{n=1}^{\infty}$ are given by (3.15) and (3.16) for $0\leqslant r<a$ and $a\leqslant r<\infty$, respectively (with, again, h replaced by $h^{(0)}$). These solutions trivially satisfy the radiation condition (4.15) since they decay exponentially rapidly at infinity.

Given that we have determined $h^{(0)}$ and $\varphi^{(0)}$, we can now evaluate the integrands in (4.12) and (4.13). After integration by parts and exploiting the radial symmetry

of $h^{(0)}$, it follows that

$$c^{(1)} = \frac{\displaystyle\int_0^{2\pi}\int_0^a \sin(\theta)\tilde{h}_r(r)\varphi^{(0)}\,|_{z=-1}\, r\,\mathrm{d}r\mathrm{d}\theta}{\displaystyle 2\pi\int_0^a \tilde{h}(r)r\,\mathrm{d}r} = 0, \tag{4.23}$$

$$\begin{aligned}\tilde{c}^{(0)} &= -\frac{\displaystyle\int_0^{2\pi}\int_0^a \cos(\theta)\tilde{h}_r(r)\varphi^{(0)}\,|_{z=-1}\, r\,\mathrm{d}r\mathrm{d}\theta}{\displaystyle 2\pi\int_0^a \tilde{h}(r)r\,\mathrm{d}r}\\ &= -\frac{\gamma\Phi_0^2(-1)\displaystyle\int_0^a \tilde{h}_r(r)J_1(\sqrt{\lambda_0}r)r\,\mathrm{d}r}{\displaystyle\int_0^a \tilde{h}(r)r\,\mathrm{d}r}\\ &= \frac{\gamma\sqrt{\lambda_0}\Phi_0^2(-1)\displaystyle\int_0^a \tilde{h}(r)J_0(\sqrt{\lambda_0}r)r\,\mathrm{d}r}{\displaystyle\int_0^a \tilde{h}(r)r\,\mathrm{d}r}\\ &= \frac{\sqrt{\lambda_0}[\gamma\Phi_0(-1)]^2}{\displaystyle\int_0^a \tilde{h}(r)r\,\mathrm{d}r} > 0.\end{aligned} \tag{4.24}$$

Thus, we conclude that there is no $O(\mu)$ correction to the along-slope translation velocity, i.e. the weakly radiating eddy travels in the along-slope direction with a velocity well approximated by the *Nof* velocity. From (4.24) we see that the generated topographic Rossby wave field leads to down-slope motion. As argued by Flierl (1984), the motion is the consequence of the wave drag exerted on the eddy by the wave field, which, through the underlying geostrophic balance, results in transverse motion. Note that the motion is toward deeper water, i.e. 'southward' thinking of the sloping bottom as a topographic β-plane and, hence, southwestward overall including the contribution associated with the Nof velocity.

To examine the parametric dependence of the cross-slope translation velocity it is convenient to be specific. Let us consider constant stratification and the parabolic eddy model (3.18). It follows that

$$\gamma = \frac{2J_2(\sqrt{\lambda_0}a)}{\lambda_0}, \qquad \Phi_0(-1) = \left(\frac{2\lambda_0}{\lambda_0 + 1 - N^2}\right)^{1/2}, \tag{4.25}$$

so that

$$\tilde{c} \simeq \frac{32\mu J_2^2(\sqrt{\lambda_0}a)}{a^2\sqrt{\lambda_0}(\lambda_0 + 1 - N^2)}, \tag{4.26}$$

where we have reintroduced the μ coefficient associated with (4.1).

The dependence of $\tilde{c}$ on the eddy radius a and the Brunt–Väisälä frequency is not monotonic. In figure 7 we plot $\tilde{c}$ versus a for $N = 1.0$, 2.0 and 5.0, respectively, assuming $\mu = 1.0$. We see that the maximum cross-slope velocity increases for increasing N, but that it is located at ever smaller a. The points where $\tilde{c} = 0$

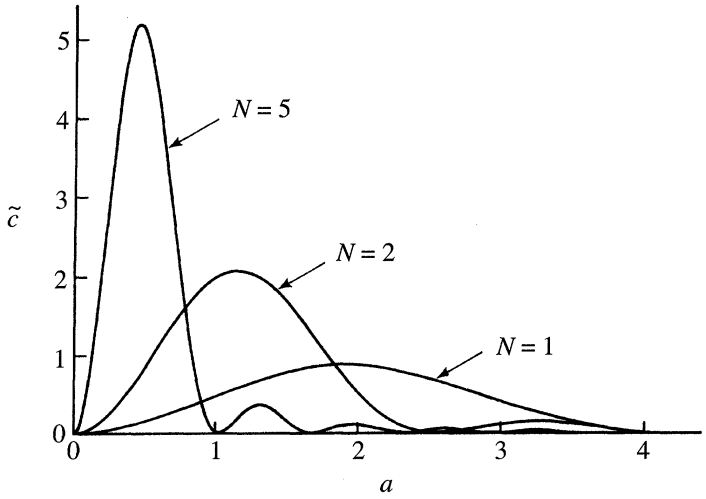

Figure 7. Graph of the cross-slope velocity $\tilde{c}$ versus the eddy radius a for $N = 1.0$, 2.0 and 5.0, respectively, with $\mu = 1.0$ as determined by (4.26).

correspond to those a values for which $J_2(\sqrt{\lambda_0}a) = 0$, i.e. those radii for which there is no topographic Rossby wave field. The dependence of $\tilde{c}$ on the height of the lower-layer cold dome is simply linear since $\mu \propto h_*$. Even though it is not formally permissible to do so, if one were to use the above result to estimate the down-slope speed of a radiating cold dome for physically acceptable values of μ, (4.26) suggests a possible dimensional order of magnitude for $\tilde{c}^*$ of the order of 5 cm s^{-1} for a cold pool with characteristics like that observed by Houghton *et al.* (1982), and as large as 15 cm s^{-1} for the pulses associated with deep-water replacement in the Strait of Georgia (LeBlond *et al.* 1991).

One reasonable objection to the above result is that it ignores the underlying time dependence associated with a radiating cold dome. The Swaters (1998*b*) description of a radiating cold dome includes time dependence in both the eddy and topographic Rossby wave field. Perhaps surprisingly, it was found that even up to second order, the time dependence does not give rise to unsteady motion in the centre of mass of the eddy, i.e. the along-slope velocity is the Nof velocity and the cross-slope velocity is given by the two-layer analogue of (4.24). Although we have not carried out the Swaters (1998*b*) calculation for the present model, we speculate that the same result holds for the continuously stratified model.

In order to illustrate the spatial structure of these radiating cold domes we will examine a radiating analogue of the parabolic cold dome described in § 3. We assume $N = \mu = 1.0$ and take $a = 3.85$ so that γ, as given by (4.18), is non-zero. In figure 8*a*, *b* we show contour plots of the upper-layer geostrophic pressure at $z = -1.0$ and 0.0, respectively. The wave field corresponds to the crescent-shaped contours to the left of the eddy. The wave field, like the eddy itself, is bottom-intensified.

As in the non-radiating case, the $\mu \approx 1.0$ solution does not transport upper-layer fluid parcels throughout the upper layer. However, for $\mu \approx 2.0$, there are closed isolines of the co-moving stream function $\mu\varphi + y$ (we hesitate to use the term streak lines since, strictly speaking, the radiating-cold-dome problem is not steady) throughout the water column, similar to that described in § 3. We do not include these contour plots here. Full details can be found in Poulin (1997).

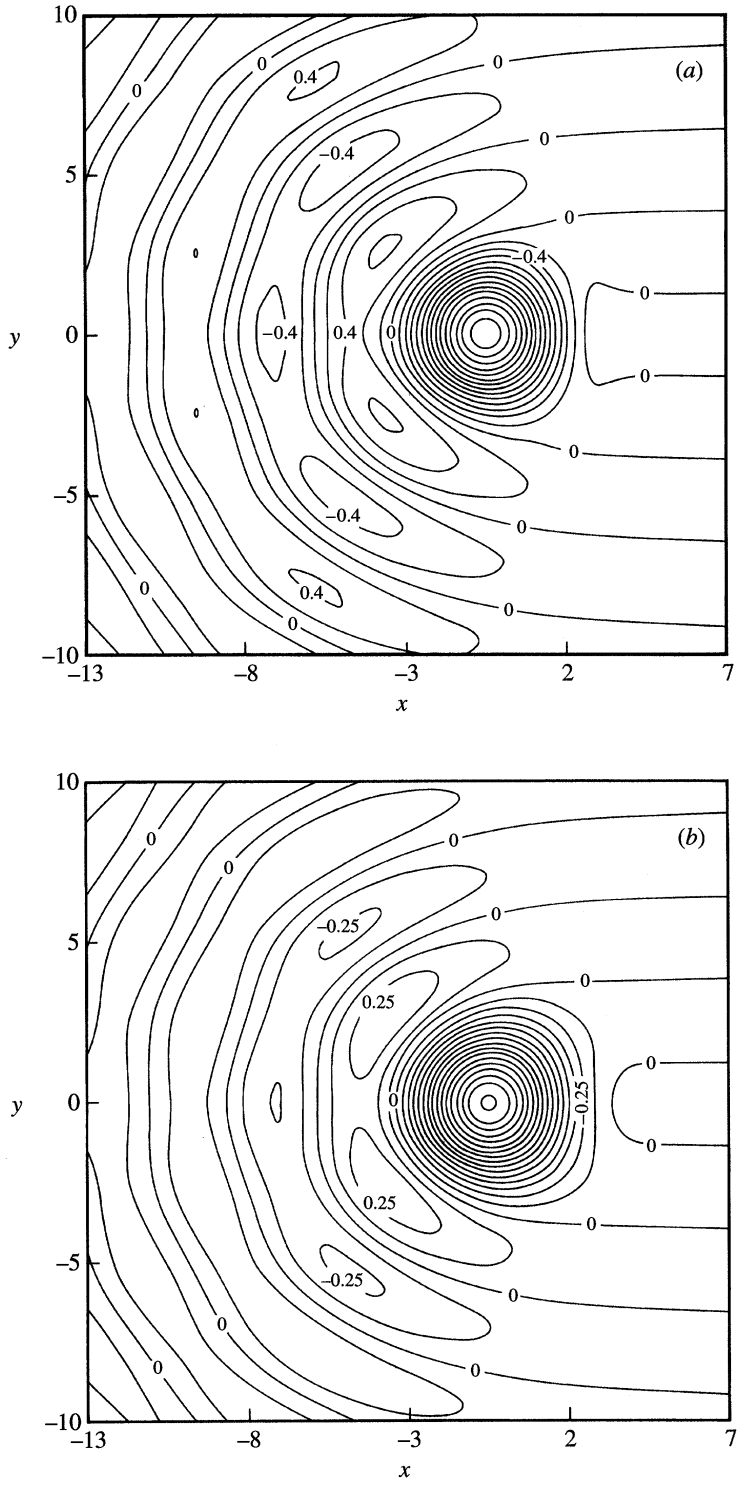

Figure 8. Contour plots of the upper-layer stream function for a radiating cold dome at (*a*) $z = -1.0$ and (*b*) $z = 0.0$. The contour interval in (*a*) is 0.2 and in (*b*) is 0.125.

5. Conclusions

We have examined the properties of eddy solutions to a new model of mesoscale gravity currents within a continuously stratified fluid overlying a sloping bottom, which we introduced in part I. A general formulation for arbitrary steadily travelling solutions was given including a variational principle. Unfortunately, it can be viewed as a consequence of Andrews's theorem that one cannot use the variational principle to establish Arnol'd-like stability of these solutions.

Two classes of eddy solutions were investigated. The first corresponded to isolated eddies. These solutions were radially symmetric and satisfied the Mory–Stern isolation constraint. This constraint completely eliminates a topographic Rossby wave field in the upper layer and leads to a quantization of the allowed eddy radius. The eddy moves in the along-slope direction with the Nof velocity and there is no cross-slope motion whatsoever. In the lower layer, the circulation is largely anticyclonic, but there is a small region of cyclonic flow, which is required to satisfy the Mory–Stern isolation constraint. In the upper layer, the flow is strictly cyclonic and is bottom intensified. For realistic values of the interaction parameter, it is possible for intermediate and near-surface water parcels to be transported in the along-slope direction.

We also constructed an approximate solution for a radiating cold dome. The topographic Rossby wave field, while bottom intensified, extends throughout the water column and is located behind the propagating eddy. The interaction between the wave field and the cold dome induces a down-slope velocity in the eddy.

This work was completed while G.E.S. was an invited participant in the Mathematics of Atmosphere and Ocean Dynamics Programme hosted by the Isaac Newton Institute for Mathematical Sciences at the University of Cambridge. Preparation of this manuscript was supported in part by a research grant awarded by the Natural Sciences and Engineering Research Council of Canada and by a Science Subvention awarded by the Department of Fisheries and Oceans of Canada to G.E.S., and by a Province of Alberta Postgraduate Scholarship awarded to F.J.P.

References

Andrews, D. G. 1984 On the existence of nonzonal flows satisfying sufficient conditions for stability. *Geophys. Astrophys. Fluid Dynamics* **28**, 243–256.

Baines, P. G. 1995 *Topographic effects in stratified flows.* Cambridge University Press.

Benjamin, T. B. 1984 Impulse, flow force and variational principles. *IMA J. Appl. Math.* **32**, 3–68.

Britter, R. E. & Linden, P. F. 1980 The motion of the front of a gravity current travelling down an incline. *J. Fluid Mech.* **99**, 531–543.

Bruce, J. G. 1995 Eddies southwest of the Denmark Strait. *Deep Sea Res.* **42**, 13–29.

Charney, J. G. & Flierl, G. R. 1981 Oceanic analogues of large-scale atmospheric motion. In *Evolution of physical oceanography—scientific surveys in honor of Henry Stommel* (ed. B. A. Warren & C. Wunsch), pp. 504–548. Cambridge, MA: MIT Press.

de Verdiere, A. C. 1986 On mean flow instabilities within the planetary geostrophic equations. *J. Phys. Oceanogr.* **16**, 1981–1984.

Flierl, G. R. 1984 Rossby wave radiation from a strongly nonlinear warm eddy. *J. Phys. Oceanogr.* **14**, 47–58.

Flierl, G. R., Larichev, V. D., McWilliams, J. C. & Reznik, G. M. 1980 Dynamics of baroclinic and barotropic solitary eddies. *Dyn. Atmos. Oceans* **5**, 1–41.

Hogg, H. G. 1980 Effects of bottom topography on ocean currents. *Orographic effects in planetary flows.* GARP Publ. Ser., no. 23, pp. 167–265.

Honji, H. & Hosoyamada, T. 1989 Instability of the rotating gravity current flow down a slope. *Rep. Res. Inst. Appl. Mech.* **35**, 55–64.

Houghton, R. W., Schlitz, R., Beardsley, R. C., Butman, B. & Chamberlin, J. C. 1982 The middle Atlantic bight pool: evolution of the temperature structure. *J. Phys. Oceanogr.* **12**, 1019–1029.

Huppert, H. E. 1975 Some remarks on the initiation of inertial Taylor columns. *J. Fluid Mech.* **67**, 397–412.

Jiang, L. & Garwood Jr, R. W. 1996 Three-dimensional simulations of overflows on continental slopes. *J. Phys. Oceanogr.* **26**, 1214–1233.

Karsten, R. H., Swaters, G. E. & Thomson, R. E. 1995 Stability characteristics of deep-water replacement in the Strait of Georgia. *J. Phys. Oceanogr.* **25**, 2391–2403.

Larichev, V. D. & Reznik, G. M. 1976 Two-dimensional Rossby soliton: an exact solution. *Rep. USSR Acad. Sci.* **231**, 1077–1079.

LeBlond, P. H., Ma, H., Doherty, F. & Pond, S. 1991 Deep and intermediate water replacement in the Strait of Georgia. *Atmos. Ocean* **29**, 288–312.

Mory, M. 1985 Integral constraints on bottom and surface isolated eddies. *J. Phys. Oceanogr.* **15**, 1433–1438.

Mory, M., Stern, M. E. & Griffiths, R. W. 1987 Coherent baroclinic eddies on a sloping bottom. *J. Fluid Mech.* **183**, 45–62.

Nof, D. 1983 The translation of isolated cold eddies on a sloping bottom. *Deep Sea Res.* **30**, 171–182.

Pedlosky, J. 1984 The equations for geostrophic flow in the ocean. *J. Phys. Oceanogr.* **14**, 448–455.

Poulin, F. J. 1997 The dynamics of mesoscale cold-pools and gravity currents within a continuously-stratified fluid overlying gently sloping topography. MSc thesis, Department of Mathematical Sciences, University of Alberta, Canada.

Poulin, F. J. & Swaters, G. E. 1999 Sub-inertial dynamics of density-driven flows in a continuously stratified fluid on a sloping bottom. I. Model derivation and stability characteristics. *Proc. R. Soc. Lond.* A **455**, 2281–2304. (Preceding paper.)

Shepherd, T. G. 1990 Symmetries, conservation laws, and Hamiltonian structure in geophysical fluid dynamics. *Adv. Geophys.* **32**, 287–335.

Swaters, G. E. 1991 On the baroclinic instability of cold-core coupled density fronts on a sloping continental shelf. *J. Fluid Mech.* **224**, 361–382.

Swaters, G. E. 1998*a* Numerical simulations of the baroclinic dynamics of density-driven coupled fronts and eddies on a sloping bottom. *J. Geophys. Res.* **103**, 2945–2961.

Swaters, G. E. 1998*b* Dynamics of radiating cold domes on a sloping bottom. *J. Fluid Mech.* **364**, 221–251.

Swaters, G. E. & Flierl, G. R. 1991 Dynamics of ventilated coherent cold eddies on a sloping bottom. *J. Fluid Mech.* **223**, 565–587.

Swaters, G. E. & Mysak, L. M. 1985 Topographically-induced baroclinic eddies near a coastline, with application to the northeast Pacific. *J. Phys. Oceanogr.* **15**, 1470–1485.

Whitehead, J. A., Stern, M. E., Flierl, G. R. & Klinger, B. 1990 Experimental observations of a baroclinic eddy over a sloping bottom. *J. Geophys. Res.* **95**, 9585–9610.